REPORT DOCUMENTATION PAGE

Form Approved
OMB No. 0704-0188

1. REPORT DATE *(DD-MM-YYYY)*	2. REPORT TYPE	3. DATES COVERED *(From - To)*
20-12-2007	Final	Jan. 2004 - Dec. 2007

4. TITLE AND SUBTITLE
Simulating Magneto-Aerodynamic Actuator

5a. CONTRACT NUMBER

5b. GRANT NUMBER
FA9550-05-1-0164

5c. PROGRAM ELEMENT NUMBER

6. AUTHOR(S)
Joseph J.S. Shang

5d. PROJECT NUMBER

5e. TASK NUMBER

5f. WORK UNIT NUMBER
666099

7. PERFORMING ORGANIZATION NAME(S) AND ADDRESS(ES)

Wright State University
3640 Colonel Glenn Hwy
Dayton, OH 45435-0001

8. PERFORMING ORGANIZATION REPORT NUMBER

9. SPONSORING / MONITORING AGENCY NAME(S) AND ADDRESS(ES)
Air Force Office of Scientific Research
875 N. Randolph Street
Suite 325
Arlington, VA 22203-1768
Dr John Schmisseur/NA

10. SPONSOR/MONITOR'S ACRONYM(S)
AFRL/AFOSR

11. SPONSOR/MONITOR'S REPORT NUMBER(S)

12. DISTRIBUTION / AVAILABILITY STATEMENT
Unclassified and unlimited distribution

AFRL-SR-AR-TR-08-0042

13. SUPPLEMENTARY NOTES

14. ABSTRACT

A hypersonic flow control by amplifying an electromagnetic perturbation through viscous-inviscid interaction has been developed and verified by experimental observations. The electromagnetic perturbation is generated by a near-surface direct current discharge. The Joule heating and Lorentz acceleration induce an oblique shock over the localized plasma domain and produce a high-pressure plateau for flow control. The interdisciplinary phenomenon has been successfully simulated by solving the three-dimensional, magneto-fluid-dynamic equations with a weakly ionized gas model based on the drift-diffusion theory. The side-by-side computational and experimental research effort has demonstrated that the magneto-fluid-dynamic interaction is an innovative and effective mechanism of the virtual leading edge strake and virtual variable cross-sectional area inlet cowls for hypersonic flow control. Technology transfer has also been accomplished through personal interaction with personnel of Air Force Research Laboratroy and NASA National Aerospace Instiute.

15. SUBJECT TERMS
Hypersonic, Plasma actuator, Flow Control, Computational Simulations

16. SECURITY CLASSIFICATION OF:			17. LIMITATION OF ABSTRACT	18. NUMBER OF PAGES	19a. NAME OF RESPONSIBLE PERSON
a. REPORT	b. ABSTRACT	c. THIS PAGE			19b. TELEPHONE NUMBER *(include area code)*
UU	UU	UU	UU	28	

Standard Form 298 (Rev. 8-98)
Prescribed by ANSI Std. Z39.18

Simulating Magneto-Aerodynamic Actuator

AFOSR GRANT FA9550-05-1-0164

J.S. Shang
Mechanical and Material Engineering Department
Wright State University
3640 Colonel Glenn Highway
Dayton Ohio 45435-0001
937-775-5094 (v) 937-775-5082 (f)
joseph.shang@wright.edu

Abstract

Partially ionized gas is a frequently encountered flow medium in most hypersonic flights. Flow control based on an additional electromagnetic force and energy of the flow medium has been innovated to achieve improved aerodynamic performance of hypersonic vehicles. However, the available energy from the weakly ionized gas for flow field modification is insufficient to achieve a first-order effect even augmented by a strong magnetic field. Nevertheless, an innovative and viable flow control mechanism has been found by using a near-surface gas discharge. The present effort demonstrates that the effect of a direct current discharge when amplified by the inviscid-viscous interaction can become an effective mechanism for hypersonic flow control. The research results from computational simulations, after being verified with experimental observations are summarized for a virtual hypersonic leading edge strake and virtual variable-area hypersonic inlet cowl.

Introduction

Direct current discharge (DCD) has been widely adopted as a hypersonic flow control mechanism [1-15]. Some of the early flow control ideas were introduced since the later 1990's by Bityurin, Kilmov, Leonov, and many others [1-3]. Macheret, Shneider, and Miles have also advocated the idea of using electron beam ionization for the control of hypersonic scramjet inlets [4]. In their approach, a simple model of a beam-generated ionization profile is used to describe the required electric conductivity for the electromagnetic force. On the other hand, a series of side-by-side computational and experimental investigations of the DCD were conducted in a hypersonic MHD flow channel by Shang, Kimmel, Menart, and Surzhikov [5-8]. An externally applied transverse magnetic field has also been implemented to enhance the flow control effectiveness. For computational simulations, a physical based non-equilibrium, two-temperature, three-component plasma model was developed based on the classic drift-diffusion theory [8]. Meanwhile, DCD applications have been extended to axisymmetric configurations by Borghi et al [9] and Cristofolini et al [10].

More recently, the near surface electric discharge has been applied to boundary layer control through hydrodynamic instability of the laminar-turbulent transition, flow separation, and shock position modification [11-15]. In most flow control applications, the magnitude of the applied electromagnetic force appears only on the level of a perturbation in comparison with the aerodynamic inertia of high-speed flow. As a consequence, the impact of flow control is relatively limited and the control effectiveness is restricted to a local domain. Two obvious remedies to increase the electromagnetic force are either applying a strong magnetic field or using a pulsed discharge. The Lorentz acceleration in plasma is well-known and its effectiveness for flow control is strongly depended on the relative orientation of the fluid motion and magnetic field polarity [14]. The advantage of a pulsed discharge is easily understood by the huge disparity in characteristic wave speeds of light and sound. A repetitively pulsed discharge can be an efficient and stable ionization source to sustain a higher electric conductivity in a nonequilibrium gas discharge [15]. These discharge enhancements also bring forth an intensive and much more complex magneto-fluid-dynamic interaction. Therefore, it is important to better understand the mechanisms and special features of the near-surface discharge for flow control.

The possible electromagnetic effects generated by the DCD are the Lorentz acceleration, electrostatic force, plasma and electrode heating; all of which have an extremely limited magnitude [8,11]. The Lorentz acceleration is significant only in the presence of an externally applied magnetic field; and due to a relative low current density the magnitude of this force is just a few kN/m^3 [16,17]. The electrostatic force is mostly detectable in the cathode layer where the substantial space charge separation occurs; its magnitude is often less than one kN/m^3 which is weaker than the pulsing force generated by either the radio frequency or dielectric barrier discharge (RFD and DBD) at atmospheric condition [18,19]. In general, the electromagnetic forces are two-order of magnitudes lower than the aerodynamic inertia of a typical hypersonic flow. In addition, the orientation of the electrostatic force is mostly downward toward the electrodes. In a thin shear layer, this force can not be supported by the shear stress and is therefore transmitted directly to the solid surface [17].

The thermal effects of the DCD include plasma and electrode heating. The former consists of mainly Joule and stochastic heating. The latter however is nearly negligible in the absence of an oscillating plasma sheath [20]. The Joule heating concentrates within the cathode layer and becomes a rather small spatial heat source to the surrounding air stream. In the electron collision process for plasma generation, the electrode heating becomes an unavoidable consequence. In a laboratory environment, these two heat fluxes have nearly the same order of magnitude, but are much smaller than the energy content of the hypersonic flow. This heat flux enters the flow field by the convective process with a magnitude less than one W/cm^2 [5,7]. Yet experimental and computational investigations have repeatedly demonstrated a significant DCD flow control effectiveness for hypersonic flows [5-8].

This phenomenon can be understood only in the light of the subsequent viscous-inviscid interaction which is also a unique feature of hypersonic flows [16,17]. In essence, the

flow displacement by a thin boundary layer is no longer negligible under the high-speed flow condition. For flow over a blunt body, the viscous-inviscid interaction is characterized by a vorticity interaction. At a sharp leading edge the pressure interaction dominates. The outward displacement triggers compression waves that coalesce into an oblique shock. The near-surface DCD becomes a driving mechanism to produce a suddenly increased displacement thickness through Lorentz acceleration with an externally applied magnetic field and heat sources in the shear layer and from the electrode surfaces. The injected thermal flux heats the surrounding air stream and lowers the density within the shear layer and leads to a sudden increased in the displacement thickness. This chain of events accentuates the pressure interaction for which the induced pressure has been successfully formulated and verified with experiments by a single classic interaction parameter, $\chi = M^3(C/Rey)^{1/2}$ [21]. This interaction phenomenon actually forms a closed feed-back loop between the growth rate of the displacement thickness and the induced streamwise pressure gradient. At the lower χ value, the grow rate is unaltered from the laminar flow ($\delta^* \sim x^{1/2}$), but changes to a three-quarter power ($\delta^* \sim x^{3/4}$) when the parameter χ exceeds the value of three. Most importantly, the magnitude of the induced pressure increases according to the cube power of the free-stream Mach number to become a viable hypersonic flow control mechanism.

In the present study, the interaction between fluid dynamics and the near-surface DCD is simulated by the magneto-fluid-dynamic equations with a drift-diffusion weakly ionized gas (WIG) model. The investigations focus on a glow discharge over the sharp leading edges of a wedge and constant cross-sectional area rectangular and cylindrical inlets. The verified simulated results of the virtual leading edge strake and virtual variable geometric inlet cowls will be presented.

Governing Equations

In most aerodynamic applications for flow control using plasma actuators the magnetic Reynolds number, $Re_m=u\sigma\mu_m L$ is often much less than unity [16,17]. According to the investigated flow condition in a hypersonic plasma channel, the Re_m has a value of 8.48×10^{-6}. Under this condition, the induced magnetic field intensity is negligible in comparison with an externally applied field. The magnetic-fluid-dynamic equations at the low magnetic Reynolds number is adopted for the present analysis [22,23].

$$\partial\rho/\partial t + \nabla\cdot(\rho\mathbf{u})=0 \qquad (1\text{-}1)$$

$$\partial\rho\mathbf{u}/\partial t + \nabla\cdot(\rho\mathbf{uu}-\boldsymbol{\tau}) = \mathbf{J}\times\mathbf{B} \qquad (1\text{-}2)$$

$$\partial\rho e/\partial t + \nabla\cdot(\rho e\mathbf{u}-\mathbf{q}-\mathbf{u}\cdot\boldsymbol{\tau}) = \mathbf{E}\cdot\mathbf{J} \qquad (1\text{-}3)$$

The governing partial differential equation system is identical to the Navier-Stokes equations except the non-zero source terms. The DCD generated under laboratory condition, has a maximum charged particle number density around 8.8×10^{11}/cc over the cathode, and the electrical conductivity is less than 1 mho/m locally [5,7,24]. At an experimental stagnation pressure of 580 Torr (7.47 Kpa) and a Mach number of 5.15, the air number density in the test section is 1.57×10^{17}/cc; thus the mass fraction of the charged particles ranges from 10^{-5} to 10^{-6} which is merely a trace amount.

The vibrational kinetics of nitrogen have been studied by Petrusev et al [25] including the excitation by electron impact, vibrational exchange, and vibrational-translational relaxation. The full fifty quantum levels of nitrogen are considered in the numerical analysis. The bulk of vibrationally excited molecules mostly take up the lower quantum states, and the level of population decreases rapidly with an increasing vibrational quantum number. It is therefore reasonable to consider only the transport properties of the weakly ionized air and to neglect the effects of nonequilibrium thermodynamics and chemical kinetics.

The physics of ionization by electron collision is very complex and involves interaction at the atomic level of the gas and solid. The electrons are produced by the avalanche growth from secondary emission. The macroscopic plasma generation process via electron collision at the microscopic scale is accurately described by Townsend's formulation [26,27]. Therefore, a rational model for a direct current discharge needs only to concentrate on the dynamics of the charged particles due to drift motion and diffusion including ambipolar diffusion [8,16,17]. These transport properties of the partially ionized plasma are independent of how the gas discharge is generated.

To model the electromagnetic perturbation, a direct current gas discharge model based on the drift-diffusion theory is incorporated. Surzhikov and Shang [8] have successfully developed a model for a three-component (neutral, electron, and ion) and two-temperature, weakly ionized gas. Poggie also adopted this model in his work for shock-wave/boundary-layer interactions for plasma flow control [28]. The basic model, including an externally applied magnetic field, can be given as:

$$\partial n_e/\partial t + \nabla\cdot\Gamma_e = \alpha(E,p)|\Gamma_e| - \beta n_+ n_e \quad (1\text{-}4)$$

$$\partial n_+/\partial t + \nabla\cdot\Gamma_+ = \alpha(E,p)|\Gamma_e| - \beta n_+ n_e \quad (1\text{-}5)$$

$$\Gamma_e = n_e\mathbf{u_e} - D_e\nabla n_e - n_e\mu_e(\mathbf{E}+\mathbf{u_e}\times\mathbf{B}) \quad (1\text{-}6)$$

$$\Gamma_+ = n_+\mathbf{u_+} - D_+\nabla n_+ + n_+\mu_+(\mathbf{E}+\mathbf{u_+}\times\mathbf{B}) \quad (1\text{-}7)$$

In the above formulation α (E, p) and β are the first Townsend ionization coefficient and recombination coefficient. The parameters μ_e and μ_+ are the electron and ion mobilities, and D_e and D_+ are the electron and ion diffusion coefficients [26,27]. When the applied transverse magnetic field is aligned with the z coordinate, the Lorentz acceleration is reduced into two components in x and y coordinates.

$$\mathbf{u_e}\times\mathbf{B} = u_{e,y}B_z\mathbf{i} - u_{e,x}B_z\mathbf{j} \quad (1\text{-}8)$$

$$\mathbf{u_+}\times\mathbf{B} = u_{+,y}B_z\mathbf{i} - u_{+,x}B_z\mathbf{j} \quad (1\text{-}9)$$

A compact formulation is achieved by introducing the Hall parameter for electrons and ions as $\beta_e = \mu_e B_z$ and $\beta_+ = \mu_+ B_z$ which are simply the ratios of the cyclotron and averaged charged-and-neutral collision frequencies [22,23]. In the presence of a transverse magnetic field of B_z, the motions of the charge particles are affected only in the plane that is perpendicular to the applied magnetic field. In practical applications to achieve the

maximum benefit of the Lorentz acceleration, the orientation of the magnetic field is applied perpendicularly to the fluid motion.

The electrical current density that appears in the governing equations, (1-2) and (1-3), is given by the difference of the charged number flux densities:

$$\mathbf{J} = e(\Gamma_+ - \Gamma_e) \tag{1-10}$$

A compatible electrical field intensity, **E**, of the discharging domain is obtained by satisfying the charge conservation equation [8]. This equation is further simplified in the globally neutral plasma by introducing an electrical potential function, $\mathbf{E} = -\nabla\phi$. The electric field potential is then the solution of the well-known Poisson equation of plasmadynamics associated with the net space charge density, ρ_e,

$$\nabla^2\phi = -\rho_e/\varepsilon \tag{1-11}$$

The initial values and boundary conditions, as well as the numerical procedure are directly usable from the cumulative knowledge of the CFD discipline [14,16,17,28]. For the velocity components, the free-stream and the no-change condition are prescribed at the entrance, far field, and exit boundaries of the computational domain respectively. The no-slip condition applies to all the velocity components on the solid surface. The piecewise isothermal condition is prescribed for the gas temperature on the model and electrode surfaces. Finally, the surface pressure is evaluated by the vanishing normal pressure gradient condition locally.

The initial values and boundary conditions of the plasma model for a numerically stable procedure have been found through a series of sustained research efforts [8,16,17,25,29]. A key element in determining the boundary conditions is specifying the electron number density on the cathode for the secondary emission phenomenon. This physical requirement is met by specifying that the normal component of the electron density flux at the cathode be proportional to its ion counterpart [8].

$$\Gamma_e \cdot n = -\gamma\Gamma_+ \cdot n \tag{1-12}$$

Numerical Procedures

All numerical results are obtained by solving the time-dependent governing equations in conservative variables. The interdisciplinary magneto-fluid-dynamic (MFD) equations, (1-1) through (1-3), and the partially ionized plasma model; equations (1-4), (1-5), and (1-11), can be cast into the flux vector form:

$$\partial\mathbf{U}/\partial t + \nabla\cdot\mathbf{F} = 0 \tag{2-1}$$

The dependent variable **U** has the components of $\{\rho, \rho u, \rho v, \rho w, \rho e, n_e, n_+, \phi\}$. The detailed description of the flux vectors, **F**, can be found in references 16 and 17, thus they will not be repeated here. In a flux-difference splitting procedure for shock capturing, the

flux vectors at the control surface are written as the solution to the approximate Riemann problem.

$$\delta \mathbf{F}_i = 1/2[\mathbf{F}(\mathbf{U}_L) + \mathbf{F}(\mathbf{U}_R) - |M_{inv}|\,(\mathbf{U}_R - \mathbf{U}_L)]_{i+1/2}$$
$$-1/2[\mathbf{F}(\mathbf{U}_L) + \mathbf{F}(\mathbf{U}_R) - |M_{inv}|\,(\mathbf{U}_R - \mathbf{U}_L)]_{i-1/2} \qquad (2\text{-}2)$$

where $\mathbf{U}_L$ and $\mathbf{U}_R$ are interpolated values of the dependent variables, ρ, ρu, ρv, ρw, and ρe at interfaces of the control volume and M_{inv} is the Jacobian matrix of the inviscid or convective terms [30].

A slope limiter is also used to control the discontinuous pressure jumps at the shock front. Time advancement is implicit to resolve the flow that has a steady state asymptote. A min-mod limiter is adopted for the present computations.

$$(\mathbf{U}_L)_{i+1/2} = \mathbf{U}_i + 1/4[(1-\kappa)\nabla + (1+\kappa)\Delta]_i \qquad (2\text{-}3)$$
$$(\mathbf{U}_R)_{i+1/2} = \mathbf{U}_{i+1} - 1/4[(1-\kappa)\Delta + (1+\kappa)\nabla]_{i+1} \qquad (2\text{-}4)$$

In the present application, the value of the parameter κ is assigned a value of 1/3 to yield a third-order upwind-biased differencing approximation. The min-mod operators are defined as:

$$\nabla = \text{minmod}\,[\nabla, (3-\kappa)/(1-\kappa)\Delta] \qquad (2\text{-}5)$$
$$\Delta = \text{minmod}\,[\Delta, (3-\kappa)/(1-\kappa)\nabla] \qquad (2\text{-}6)$$

The spatial discretization involves a semi-discrete finite-volume scheme [30,31]. The upwind-biasing approximation is applied to the convective and pressure terms. The central differencing is used for the shear stress and heat transfer terms of the governing equations.

All numerical simulations either for virtual leading-edge strake or virtual variable rectangular cross-sectional area inlet cowls are three-dimensional. The virtual variable cylindrical inlet is simulated by the axisymmetric formulation. For each group of numerical simulations, a typical two mesh system was used. For example, two mesh systems of (85× 45×81) and (105×57×101) were used for the simulation of the rectangular inlet. For convergence acceleration, three-level mesh sequencing of the multigrid technique is applied [31]. The mesh systems of the half (41×23×43) and quarter (21×12×22) mesh number densities are used for the coarser mesh computations. The data processing rate on a 400 MHz SGI Octane2 workstation is 61.6×10^{-6} seconds per cells per iteration. The convergent criterion of the present analysis is preset at a value of 3.0×10^{-7} for the normalized global residue.

MFD Flow Control Mechanism

Hypersonic flow control utilizing the magneto-fluid-dynamic (MFD) interaction is based on the intrinsic characteristic of the hypersonic similitude parameter of $M\tau$. Any small flow deflection in a supersonic or hypersonic stream will automatically trigger an oblique shock and generate a high pressure region over the disturbance. When a DCD is activated, a low density domain is created immediately adjacent to the discharging electrodes, especially over the cathode. This local expansion leads to a sudden increase of the displacement thickness of the shear layer which in turn deflects the flow away from the solid surface.

This phenomenon is easily observed in Figure 1. The numerical result is generated for the flow condition identical to an experimental effort in a hypersonic MHD channel at a Mach number of 5.15 and a Reynolds number of 2.56×10^5 based on the model length. The DCD is maintained by an applied electrical potential of 860 V and the distance between the embedded electrodes is 2.80 cm. The cathode is placed upstream of the anode at a distance of 2.48 cm from the leading edge. From the computed result, the intensive heat transfer at the edges of the discharge electrodes is clearly and correctly displayed. The Joule heating is concentrated mostly over the cathode; this result is fully substantiated by the experimental observation [5,7].

Figure 1. Temperature contours over DCD on a wedge surface

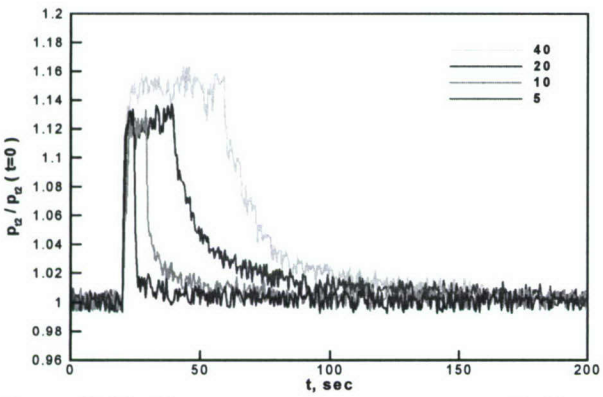

Figure 2. Surface pressure measurements during actuated DCD, EMF=1.2 kV, M=5.15, p=0.59 Torr, T=43 K

Figure 2 presents the time-trace records of the surface pressure over a sharp-leading-edge plate with embedded electrodes in a MHD flow channel. At the free-stream Mach number of 5.15, the static pressure is 0.59 Torr and the static temperature is 43 K. The DCD is actuated after the flow is established within the MHD channel. The MFD interaction is shown to generate a high pressure plateau over the cathode. The surface pressure repeatedly rises in a milliseconds time frame when the DCD is actuated and increases to a value exceeding 15% of that of the deactivated counterpart [7]. The data were recorded for a sampling period from 3 to 40 seconds. At a longer duration of activations, the pressure plateau continuously increases because the electrode heating also contributes to the thickening of the boundary-layer displacement thickness [5].

The small electromagnetic perturbation is amplified by the classic hypersonic viscous-inviscid interaction. The amplification becomes optimum when the perturbation is placed as close as possible to the sharp leading edge. According to the theory of pressure interaction, the induced surface pressure can be derived from the tangent-wedge or tangent-cone approximation and the surface pressure is described by a single parameter, $\chi = M^3(C/Rey)^{1/2}$ [21]. At a typical operational condition of the MHD channel, the value of χ is 0.69 at a downstream distance of 10 cm from the leading edge of the model. The comparisons of the classic pressure interaction theory and the solutions of the compressible Navier-Stokes equations at Mach numbers around five and ten are given in Figure 3. The agreement between the theory and numerical simulations is excellent and the strong dependence of the induced surface pressure to the free-stream Mach number is also clearly revealed.

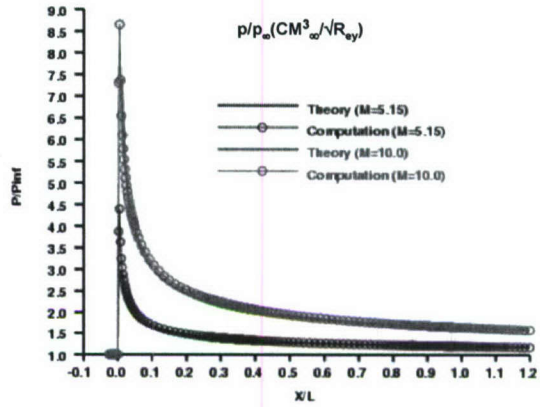

Figure 3. Pressure interaction at hypersonic leading edge, $\chi = CM_\infty^3/\sqrt{R_{ey}}$

In summary, flow control using a direct current discharge is derived from the electromagnetic perturbation and amplified by the hypersonic pressure interaction. The interaction parameter is a function of the inverse square root of the Reynolds number based on the running length from the leading edge and is also proportional to the cube power of the free stream Mach number [21]. Based on this theory, the viscous-inviscid interaction is dominant near the leading edge and the pressure rise increases strongly with the oncoming Mach number.

Validating the WIG Model

All experimental data were collected in a MHD channel. This hypersonic low-density facility of the Air Force Research Laboratory is a blow-down, free-jet facility. It is designed to deliver a nominal Mach 5 flow in the test section with a diffuser that achieves at least a normal shock recovery. The simulated altitude based on the value of flow density spans a range from 30,000 to 50,000 m. The entire length of the plasma channel is 155.5 cm and the tunnel exhausts to a 2800 m^3 vacuum sphere. At a fixed stagnation temperature of 270 K, the channel has an operational stagnation pressure range from 0.1 to 1.0 atm [5-7,32,33]. At a typical stagnation pressure of 560 Torr (74.7 kPa), the free-stream in the test section has a velocity, density, and temperature of 675.5 m/s, 0.0096 kg/m^3, and 43 K, respectively. Under these conditions, the unit Reynolds number in the test section is 2.44×10^6 per meter.

The detailed behavior of a draft-diffusion DCD model has been investigated continuously [8,16,17,25,27-29] and has attained good agreement with the classic results of von Engel et al [26]. In here, the partially ionized gas model will be evaluated at the experimental conditions and in an application environment. All the following presentations focus on validating the DCD model at hypersonic flow conditions of the MHD channel. In other words, the comparison of the model and measured data is conducting at static pressures from 0.59 to 0.93 Torr, a static temperature of 43 K, and a jet stream moving at 675.5 m/s.

In Figure 4, the computed global characteristics of the DCD are compared with experimental observations in a uniform transverse magnetic field from -0.05 to 0.05 Tesla [5,7,24]. The discharge is sustained by an electric potential around 840 V and a current less than 100 mA. For numerical simulations, the Hall parameters for electrons and ions are 0.44 and 0.0145 respectively. In a side-by-side electrode arrangement, the cathode is placed upstream (on the left) of the anode and with a separation distance of 3.81 cm. The

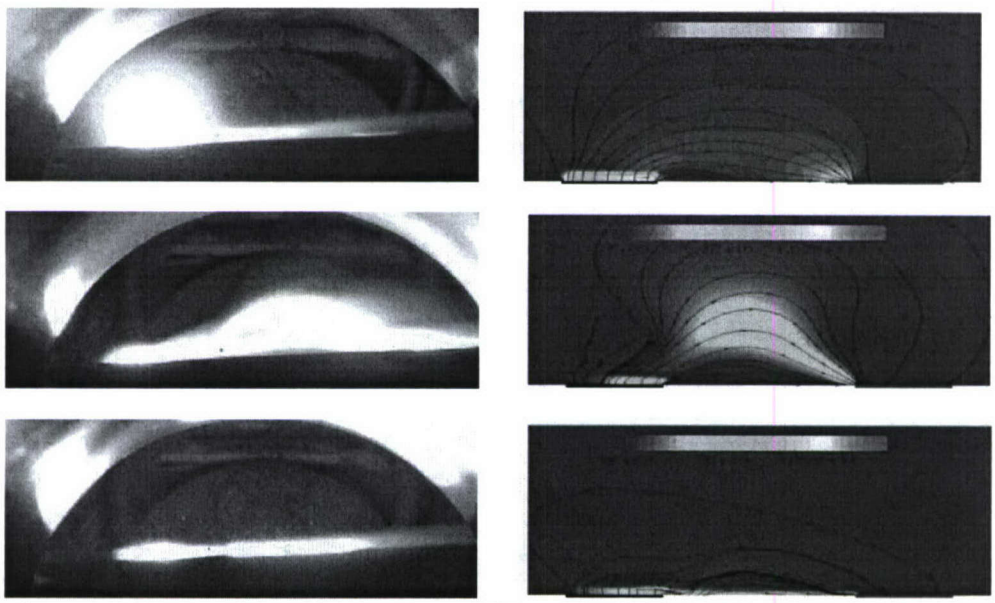

Figure 4. Simulate DCD in Transverse Magnetic field, -0.05 < B < 0.05 Tesla, EMF= 2.4 kV, p=5.0 Torr, (From top to Bottom; B=0.0 T, B=-0,05 T, and B=+0.05 T)

essential physics of the DCD is captured by the drift-diffusion model; the intensive glow associated with the transition of charged particles is duplicated by the computational simulations. Most importantly, the dominant effect of Lorentz acceleration stands out. The positive transverse field, B=+0.05, generates a suppressing force to restrain the upward movement of the electrons which is displayed in the bottom row of the figure. When the polarity is reversed, B=–0.05, the computational result in the middle row exhibits an opposite pattern. The Lorentz force under this condition expels the electrons away from the electrodes. In essence, the physically based model with a transverse magnetic field duplicates the essential discharge physics. The specific quantification of the Lorentz force to the DCD will be discussed in a later section.

The specific comparison of charge particles profile with experimental data is depicted in Figure 5. The glow discharge is maintained by an electrical field of 1.2 kV with an ambient pressure of 0.59 Torr (78.4 Pa). The studied side-by-side electrode configuration is identical to that for investigating the Lorentz force. It is well-known, that charge separation takes place in the cathode layer and the ion number density can be as high as three times or more than the electron density. The computed ion number density distribution above the anode has excellent agreement with experimental data [16,17]. The computed ion and electron number density beyond the cathode and anode layer is $9.8\times10^{9}/cm^{3}$ and correctly reflects the globally neutral property of the plasma. There is a large discrepancy between computational and experimental results for the ion number density profile directly above the cathode. However, the accuracy of measurements can be challenged, because it was collected in a supposedly globally neutral domain. Nevertheless, the difference between results is confined within one order of magnitude which is the state-of-the-art norm for the measurement disparity between data obtained by Langmuir probes close to the cathode in a high speed flow environment [5,7].

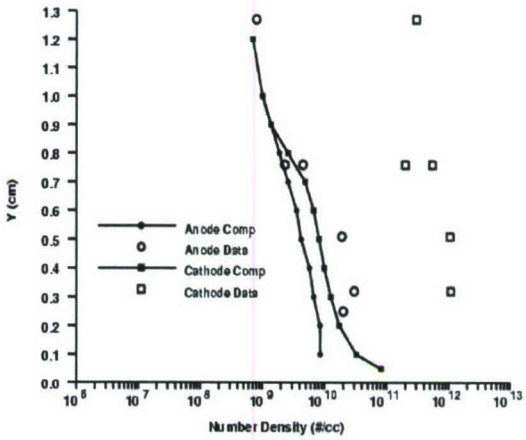

Figure 5. Validate charged particles density with data, E= 800V, p=0.97 Torr, M=5.15, T=43 K

The simulation using the drift-diffusion model also produces a reasonable agreement with measurement obtained by a stagnation temperature probe [7]. In Figure 6, the comparison is given in a dimensionless value normalized by the free-stream temperature (43 K). The size of the sheltered probe and its aerodynamic interference prevents accurate measurements within both the cathode and the anode layers. The most outstanding feature of the computational results is that the Joule heating is dominant. The gas temperature near the wall is actually higher than the surface temperatures of the cathode and anode. In fact, the cathode has attained a temperature that exceeds 460 K and mostly by the electrode heating [5-7].

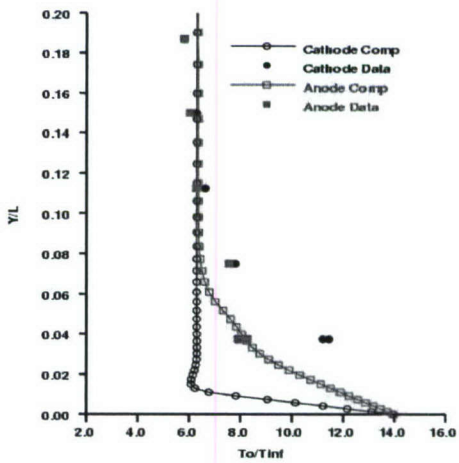

Figure 6. Verify stagnation temperature profile with data, M=1.5, Rey=2.57×10^{5}, T=43K, P=0.56 Torr, PG=64W

From previous evaluations with the classic parallel electrode configuration by von Engel et al [8,26] and the present validating process [16,17], the drift-diffusion model has demonstrated the ability in describing the essential physics of a DCD for flow control. Additional validation of the discharge physics is still required in the future.

Virtual leading-edge strake

In Figure 7, the DCD over a sharp leading edge wedge in a Mach 5.15 hypersonic stream is displayed. The near-surface plasma is generated by two electrodes embedded in the flat plate surface of the wedge. A total electrical current of 50 mA is maintained by an applied electric field of 1.2 kV in the external circuit. The maximum electron number density of the plasma is $3\times10^{11}/cm^3$, and the electrode temperature is estimated to be 460 K [5,7,24]. At an ambient pressure of 0.59 Torr and a static temperature of 43 K, the air density is $1.33\times10^{17}/cm^3$; the degree of ionization is 2.25×10^{-5} and the electrical conductivity is on the order of 1 mho/m. In this sense, the glow discharge provides a truly weakly ionized gas over the electrodes.

Figure 7. DCD over a wedge M=5.15, Rey=2.57×10^5, P=0.56 Torr, T=43K

The relative importance of the surface convective and volumetric Joule heating is confirmed by experimental and computational results. In Figure 8, solutions of the magneto-aerodynamic equations using the drift-diffusion model are compared with measurements at the Mach number of 5.15 and Reynolds number of 2.57×10^5. Numerical results were generated on the flat surface of the wedge model with the actuated DCD and the electrode heating only conditions. All of which exhibit reasonable agreement with data. Most important, the glow discharge induces a bona fide electro-aerodynamic interaction that is not possible with electrode heating alone. At a very low level power of 50 watts, the electro-aerodynamic interaction generates a pressure rise on the wedge surface is equivalent to one-degree angle of attack of the surface at Mach number of 5.15. From this result, and a series of experiments at

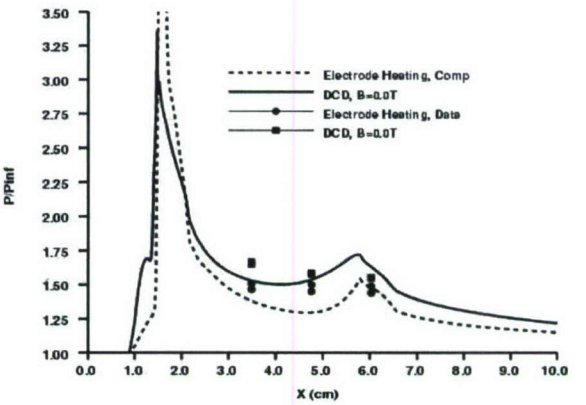

Figure 8. Surface pressure distribution over wedge with/without DCD, M=5.15, Rey=2.57×10^5, P=0.56 Torr, T=43K

increasing plasma power input, a scaling of power required for the plasma actuator per electrode area is about 9.17 watts/cm^2/degree.

The effect of the Lorentz force is easily detected from the computed surface pressure over the electrodes in Figure 9. The computed results were generated at a typical running condition of the MHD channel; the stagnation pressure and temperature of 580 Torr (74.1 kPa) and 270 K respectively. The Lorentz force is relatively small about ±0.02 N/m^3 at the externally applied uniform magnetic field of ±0.2 Tesla. The computed result generally over predicts the pressure measurement, and the measured data also exhibits an unusually large data scattering due to the unstable glow discharge in the presence of an applied magnetic field. The expelling Lorentz force (**J**×**B**<0, B=–0.2 Tesla) indeed pushes the charged particles away from the electrodes and increases the collision for momentum transfer. Thereby, the induced surface pressure is greater than the MFD interaction without the presence of a transverse magnetic field, but at identical electric field intensity. The trend of increasing the discharge domain is reversed with the opposite magnetic polarity (**J**×**B**>0, B=+0.2 Tesla). The induced surface pressure is also diminished accordingly by suppressing the outward deflection of the streamline. It is interesting to note an increased effort was required for maintaining the computational stability. Nevertheless, the numerical results using the drift-diffusion model capture the difference between the applied magnetic fields of opposite polarities.

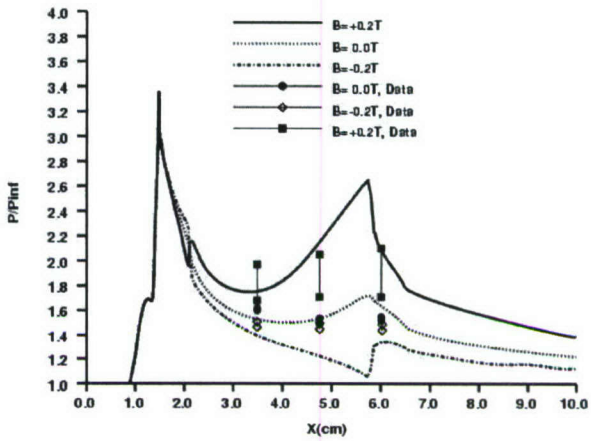

Figure 9. Surface pressure distribution with DCD and transverse magnetic field, M=5.15, Rey=2.57×10^5, P=0.56 Torr, T=43K

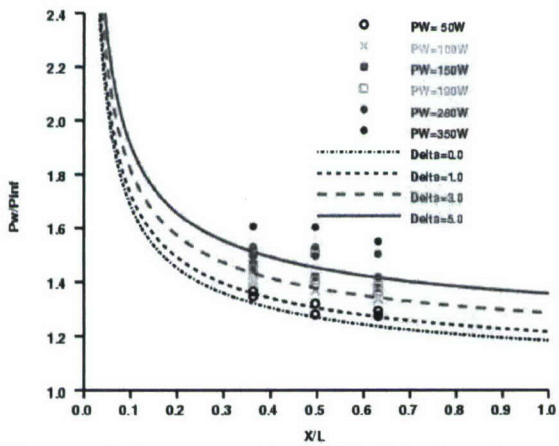

Figure 10. Power scaling of DCD virtual leading edge strake, M=5.15

The validated numerical simulations also illustrate the profound influence of a relatively small applied magnetic field to the flow control effectiveness. In fact, a transverse magnetic field of 0.2 Tesla aligning with the reverse direction of the z coordinate has generated a 34% higher pressure level on the control surface than that without the externally applied magnetic field. The control effectiveness is greatly enhanced by the Lorentz force.

The magneto-fluid-dynamic interaction produces a high pressure region between the electrodes. The high surface distribution over the immobile wedge with an activated DCD acts as if the surface had executed a pitching motion – the performance identical to a movable leading edge strake. A series of calculations with the discharge current from 50 to 350 mA yield the equivalent angles of attack from one to exceeded five degrees for the deployed virtual strake. The computed results are substantiated by experimental data depicting in Figure 10.

Virtual variable geometrical inlet cowls

The magneto-fluid-dynamic interaction is equally applicable as a virtual variable geometrical inlet cowl using the amplified electromagnetic perturbation. Computational and experimental efforts for the constant cross-sectional area rectangular and cylindrical inlets were carried out. These two inlets are designed for nearly identical cross-sectional area and the same total length to assess the relative merit of the improved aerodynamic performance and for the difference between a three-dimensional and an axisymmetric configuration.

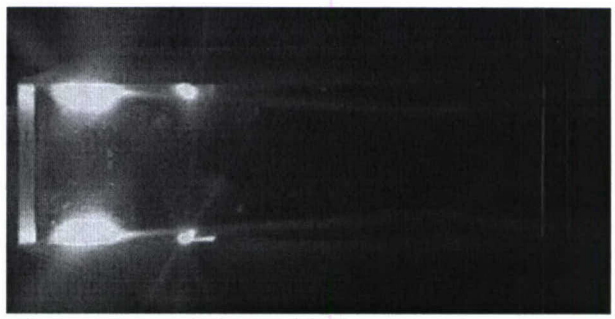

Figure 11. DCD from side-by-side Electrodes of a rectangular inlet M=5.15, Rey=2.57×10^5, P=0.56 Torr, T=43K, PG=64W

The top view of the discharge pattern with the side-by-side electrode is presented in Figure 11. The four embedded electrodes have the same dimensions of 2.03 cm^2 and the cathodes are placed at 0.64 cm from the inlet leading edge upstream to the anode. The separation distance between electrodes is 2.22 cm. At the static pressure of 0.56 Torr, the discharges are maintained at electric potentials from 600 to 800 V with electric current from 40 to 80 mA. Therefore, the electric current density has a value of 21.8mA/cm^2 over the anode and the near-surface plasma is generated by a total power input of 64 Watts within the hypersonic inlet.

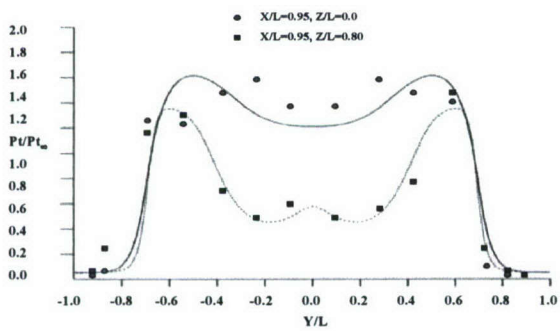

Figure 12. Comparison of Pitot pressure profiles at exit plane of rectangular inlet, M=5.15, Rey=2.57×10^5, P=0.56 Torr, T=43K

The induced shock structure by the DCD is rather complex; the mutually perpendicular leading edge and the embedded electrodes generate four oblique shocks over the inlet surface. Immediately downstream of the electrodes, a total of eight triplet points of the intersecting oblique

shocks are detected by both computational and experimental means [32]. The interacting flow field is simulated by solving the MFD equations on two mesh systems of (85×45×81) and (105×57×101). However, the major portions of the results are generated on the fine mesh and with a three-level multi-grid sequence for convergence acceleration. The oblique shock waves eventually intersect each other, reflected from the side walls, and finally dissipated [32]. For the rather complex MFD induced compression, the computational results duplicate the interacting phenomenon as shown in Figure 12. The comparison of the computed and measured Pitot pressure profiles on the center plane and at an off-set distance of z/L=0.80 has a reasonable agreement near the exit of the inlet. At this location, the MFD induced oblique shocks from the side-wall discharge are still predominant.

The density contours in the x-y plane of the rectangular inlet are given in Figure 13. It can be easily seen that the DCD strengthens the oblique shock which originated from the viscous-inviscid interaction at the sharp leading edges of the inlet. The oblique shocks from the sidewalls intersect each other at x/L=0.60 upstream to that of the weaker oblique shocks originating from the top and bottom surfaces [32]. The MFD compression is the consequence of the Joule and electrode heating that alters the boundary-layer displacement thickness on the side walls. An estimated total of 12 watts of the power used for plasma generation is converted into Joule heating; this value is in general agreement with the estimate by nonequilibrium chemical kinetics including energy cascading between the internal degrees of freedom of the weakly ionized gas [23,25].

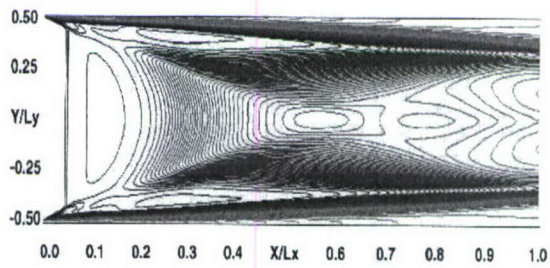

Figure 13. Joule heating distribution, M=5.15, Rey=2.57×10^5, P=0.56 Torr, T=43K, φ=800V, I=60 mA

Figure 14 presents the comparison of experimental and computed Pitot pressures along the centerline of the rectangular inlet when the DCD is either activated or deactivated. Both results generated at a stagnation pressure of 580 Torr have captured the interacting oblique shocks within the inlet [32]. When the DCD is actuated, the induced oblique shock becomes steeper and moves the interception of the shock waves upstream. The ensured expansion follows the strengthened shock and produces a slightly lower Pitot pressure along the centerline

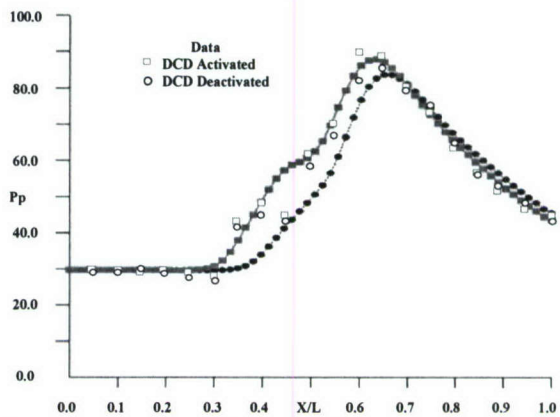

Figure 14. Comparison of Pitot pressure along centerline of rectangular inlet, M=5.15, Rey=2.57×10^5

downstream. The actuated DCD leads to a higher peak Pitot pressure and an upstream movement in contrast to its deactivated counterpart. The computed results have good agreement with the experimental data. The computations underpredict the peak Pitot pressure by 2% and overpredict the uniform entrance condition by 1.2%. This small discrepancy in magnitude is directly attributable to the fluctuating DC discharge and the uncertain Mach number at the entrance of the inlet due to model blockage.

Figure 15 presents the comparison of computed static pressure distributions in the x-z plane near the inlet exit. The difference in pressure distributions with and without the activated DC discharge is similar to that in the x-y plane, except the pressure level is consistently higher by the induced vertical sidewall compression over most of the inner core region. Since the electrodes are embedded in the vertical sidewalls, there is no additional compression from these horizontal surfaces. The increased static pressure is the result of the MFD interaction originating from the entrance of the inlet. The averaged static pressure over the entire exit cross-sectional area is 11.7% percent greater than the counterpart without electromagnetic perturbation.

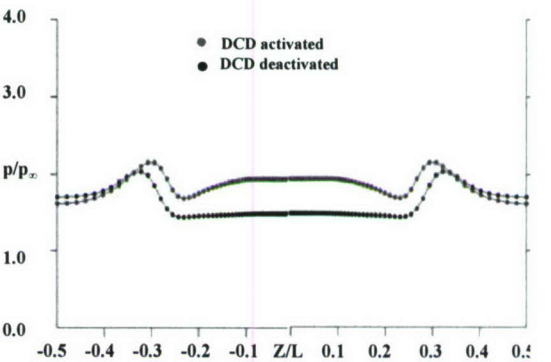

Figure 15. Static pressure profiles in x-z plane near inlet exit with/without DCD

The effectiveness of MFD compression in a constant area rectangular inlet at different free-stream Mach numbers is depicted in Figure 16. Four numerical simulations are included at the Mach number of 5.0 and 6.0; the actuated DCD produces a greater compression than the deactivated flows. At a higher Mach number, the energy input for plasma generation is kept at the same value as that for the lower Mach number flow. At the higher free-stream velocity, 810.6 m/s versus 675.5 m/s, energy is more dissipated into the air stream. Therefore, the electromagnetic perturbation is diminished and as a consequence the MFD compression is not increased according to the cube power of the Mach number. However, a higher compression can be recovered by increasing the electric current density of the DCD.

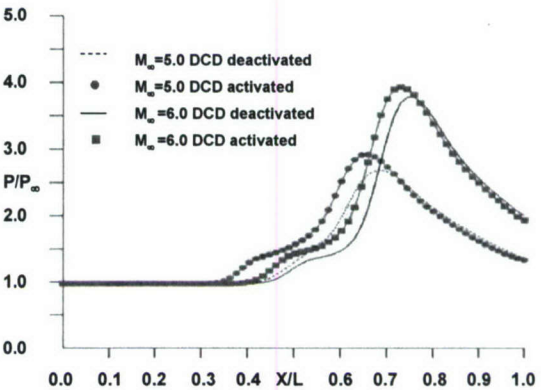

Figure 16. MFD compression at different Mach numbers, Rey=2.57×10^5, PG=64W

The photograph of the ignited DC discharge in the cylindrical inlet is presented in Figure 17. The discharge is sustained by an applied electric potential of 460 V and a current of 150 mA. The DCD is viewed from the inlet exit and at an oblique angle from the axis. The dominant visual feature of the discharge is the glow over the electrodes and the reflection from the model sidewalls. Under this testing condition, the discharge current density on the anode is 6.78 mA/cm^2; this value is nearly three times lower than that of the rectangular inlet with a different electrode arrangement [32,33]. For this reason, the DC discharge pattern of the cylindrical inlet is essentially fluctuation free. This behavior persists even when the circuit current density on the anode reaches a value of 20.34 mA/cm^2 by increasing circuit current to 150 mA. For this reason, the experimental measurements of this configuration have a significantly reduced data scatter than the previous results for a rectangular inlet [32].

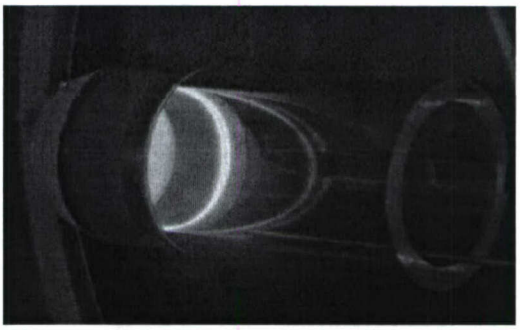

Figure 17. DCD over the leading edge of cylindrical inlet model, M=5.15, Rey=2.58× 10^5, p=0.96 Torr, PG=69 W

The density contours of the deactivated and the actuated DCD in the constant cross-sectional area cylindrical inlet are presented in Figure 18. The cylindrical inlet has an inner diameter of 3.50 cm and is designed to have a comparable cross-sectional area to the rectangular inlet of 11.8 cm^2. The entire flow field is dominated by a convergent and divergent conical shock which is induced by the pressure interaction at the leading edge. The comparative study consists of two computed results, on the lower half plane is the baseline case with the deactivated DCD and on the upper half plane the solution is generated with the actuator powered by 69.0 watts; the applied electric field potential is 460 volts and the circuit current is 150 mA. The induced shock now possesses a significant strength so that the oblique shock continues after the shock focus impinges on the inner surface of the inlet model. At a lower Reynolds number condition, Rey=1.66×10^5, the impinging shock generates an unexpected and additional shock-boundary-layer interaction near the exit. The numerical simulation shows that the adverse pressure gradient even triggers incipient flow separation near the exit plane. Unfortunately, this result is not directly verifiable by the experimental observations [33].

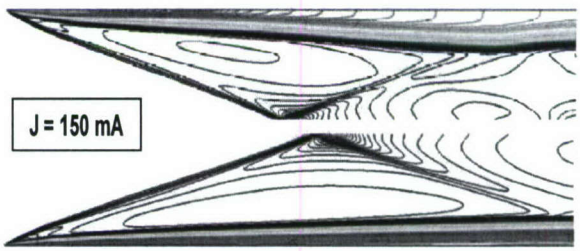

Figure 18. Density contours of the cylindrical inlet with/without the activated DCD, M=5.15, Rey=2.58× 10^5, p=0.96 Torr, T=43K, φ=480, I=150 mA

At the Reynolds number of 2.57×10^5, this specific phenomenon is further verified in Figure 19 by the comparison of the streamwise Pitot pressure distributions along the axis of the model. The computed and measured results of the actuated DCD are designated by the solid line and filled square symbols and by the dash line and the filled circles for the unperturbed condition. The computing simulations do not include the slightly blunt leading edge, thus have a weaker oblique shock. As a consequence, the shock focus is consistently formed downstream of the experimental observation. More importantly, the divergent conical shock, after passing through the shock focus, does not impinge on the inlet side wall. However the shock of the experiments impinges on the side wall and creates an adverse pressure gradient near the inlet exit which has induced an incipient flow separation and unsteady flow at the same Reynolds number condition. This behavior is different from the numerical simulations of the cylindrical inlet with a sharp leading edge in which the divergent shock exits the inlet uninterrupted.

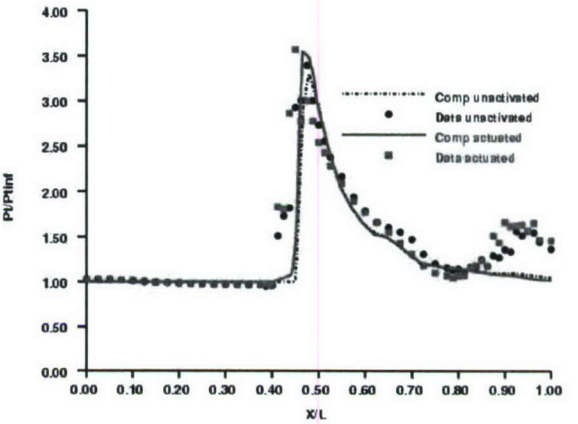

Figure 19. Impact pressure distributions along the axis of the cylindrical inlet, M=5.15, Rey=2.58×10^5, p=0.96 Torr, T=43K, φ=480, I=150 mA

The important comparison of Pitot pressure profiles near the cylindrical inlet exit plane is prevented by the unsteady or separated flow behavior at the inlet exit. In Figure 20, two sets of data taken on different days are presented together with computing results at a streamwise location of X/D=3.8; the inlet exit. The computational simulations with and without DCD actuation are embedded within the data bands. From the computational investigation and verified experimental data on the virtual inlet cowl, the DCD in a rectangular inlet has produced an additional MFD compression of 11.7% than the unperturbed counter part. The DCD in the cylindrical

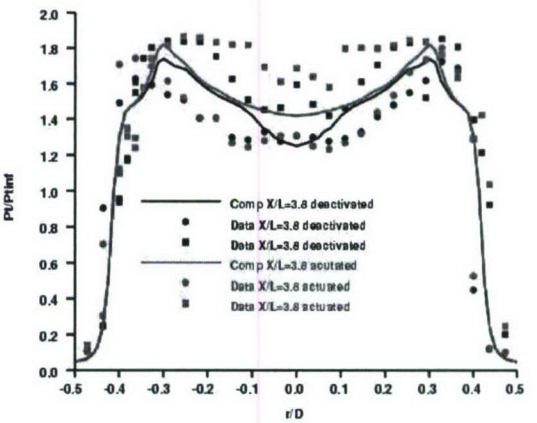

Figure 20. Pitot pressure profiles at exit of the cylindrical inlet, M=5.15, Rey=2.58×10^5, φ=480V, I=150 mA

inlet produces less compression, 6.7% under the identical free-stream conditions at a Mach number of 5.15 and the Reynolds number of 2.57×10^5. The lower compression has two distinct contributors; first the electric current density is much lower in the electrode configuration for the cylindrical inlet. Second, the intrinsic difference in spatial dimension plays a role for the difference between the rectangular three-dimensional and the axisymmetric configuration. In that, the Mangler scale of $\sqrt{3}$ actually reduces the outward displacement thickness of the electromagnetic perturbation. In summary, the DCD generate a lower MFD compression for the axisymmetric inlet, the MFD compression is generated at low power for plasma generation, 2.8 W/cm^2.

Concluding Remarks

A viable application of plasma actuators for flow control in the hypersonic regime has been demonstrated by computational analysis using the magneto-fluid-dynamic equation in the low magnetic Reynolds number limit with a plasma model. The key mechanism of an effective plasma actuator for flow control is the amplification of an electromagnetic perturbation by the unique hypersonic pressure interaction. The basic approach introduces a direct current discharge near the sharp leading edges of the inlet, thereby altering the slope of the shear layer thickness which results in a stronger viscous-inviscid interaction. This conclusion is fully substantiated by experimental observations.

In application as a virtual leading edge strake, the magneto-fluid-dynamic interaction creates a pressure plateau on a fixed surface that is equivalent to a movable control surface pitching up to five degrees at the free-stream Mach number of 5.15. An externally applied transverse magnetic field increases the surface pressure rise by a factor of 1.34. The effectiveness of the virtual leading edge strake is reflected by an averaged power scaling of 9.17 watts/degree/cm^2.

The magneto-fluid-dynamic compression performs equally well as a virtual cowl that enhances the performance of constant cross-section inlets. Under the investigated condition of Mach 5.15 and Reynolds number of 2.57×10^5, the magneto-fluid-dynamic sidewall compression within a rectangular inlet produces 11.7% gain by a plasma generating power input of 4.4 watts/cm^2 from electrodes. In this aspect, the present approach using a plasma actuator for hypersonic flow control has overcome the fundamental inefficient ionization process.

The numerical results also show that the effectiveness of a virtual variable geometry cowl can increase with higher free-stream Mach number, if the intensity of the DC discharge can be sustained. Detailed and optimal electrode placement in the inlet becomes pivotal for a versatile and widely applicable virtual inlet cowl. Research efforts in this area shall be continued.

The induced magneto-fluid-dynamic compression in a cylindrical inlet is determined to be 6.7% over that of the unperturbed counterpart. The reduced compression in comparison with the three-dimensional inlet is mainly due to the reduced electric current density (6.25 mA/cm^2) of the DCD and the Mangler effect of the axisymmetric

configuration. Under this circumstance, the MFD compression gain is achieved without any loss of the stagnation pressure by the virtual variable inlet cowl.

Acknowledgment

The support by Dr. F. Fahroo and Dr. J.D. Schmisseur of AFOSR is deeply appreciated. The author is thankful for the fruitful exchange and earnest support by Dr. D. Gaitonde, Dr. R. Kimmel, and Mr. J Hayes of Air Force Research Laboratory, as well as, my colleague at Wright State University Dr. J. Menart and Prof. G. Huang. Finally but not the least, I value highly my collaboration with Prof. S. Surzhikov of the Russian Academy of Science, Moscow.

References

1. Bityurin, V., Kilmov, A., Leonov, S., Lutsky, A, Van Wie D., Brovkin, V., and Kolesnichenko, Yu., Effect of Hetrogenous Discharge Plasma on Shock Wave Structure and Propagation, AIAA 99-4940, Norfolk VA, Nov.
2. Leonov, S., Bityurin, V., Savelkin, K., and Yarantsev, D., Effect of Electrical Discharge on Separation Processes and Shock Position in Supersonic Airflow, AIAA 2002-0355. Reno NV, January 2002.
3. Bityurin, V.A., Bocharov, A.N., and Lineberry, J.T., Results of Experiments on MHD Hypersonic Flow Control, AIAA 2004-2263, Portland OR, June 2004.
4. Macheret, S.O, Shneider, M.N., and Miles, R.B., Magneto-hydrodynamic Control of Hypersonic Flow and Scramjet Inlets using Electron Beam Ionization, AIAA J. Vol. 40, No.1, 2002, pp.74-81.
5. Menart, J., Shang, J., Kimmel, R, and Hayes, J., Effects of Magnetic Fields on Plasmas Generated in a Mach 5 Wind Tunnel, AIAA 2003-4165, Orlando FL, 23-26 June 2003.
6. Shang, J.S. and Surzhikov, Magneto-Fluid-Dynamics Interaction for Hypersonic Flow Control, AIAA 2004-0508, Reno NV, January 2004.
7. Kimmel, R., Hayes, J., Menart, J., and Shang, J., Effect of Surface Plasma Discharges on Boundary Layer at Mach 5, AIAA 2004-0509, Reno NV, January 5-8, 2004.
8. Surzhikov, S.T. and Shang, J.S. Two-Component Plasma Model for Two-Dimensional Glow Discharge in Magnetic Field, J. Computational Physics, Vol. 199, 2, Sept. 2004, pp. 437-464.
9. Borghi, C.A., Carraro, M.R., and Cristofolini, A., An Axisymmetric Hall Configuration for MHD Interaction in Hypersonic Flows, AIAA 2005-4785, Toronto Canada, June 2005.
10. Cristofolini, A., Borghi, C.A., Carraro, M.R., Neretti, G., Biagioni, L., Fantoni, G., and Passaro, A., Experimental Investigation on the MHD Interaction around a Sharp Cone in an Ionized Argon Flow. AIAA 2006-3075, San Francisco CA, June 2006.
11. Bletzinger, P., Ganguly, B.N., Van Wie, D., Garscadden, A., Plasma in High-Speed Aerodynamics, J. of Physics D: Applied Physics, Vol. 38, 2005, pp. R33-57.

12. Leonov, S.B., Yarantsev, D.A., Gromov, V.G., and Kuriachy, A.P., Mechanisms of Flow control by near-surface Electrical Discharge Generation, AIAA 2005-0780, Reno NV, January 2005.
13. Leonov, S.B., Yarantsev, D.A., and Soloviev, V.R., Experiments on Control of Supersonic Flow Structure in Model Inlet by Electric Discharge, AIAA 2007-3890, Miami FL., June 2007.
14. Gaitonde, D.V., Simulation of Local and Global High-speed Flow Control with Magnetic Fields, AIAA 2005-0560, Nero NV, January 2005.
15. Nishihara, M. Jiang, N., Lempart, W.R., Adamovich, I.V, and Gogineni, S., MHD Supersonic Boundary Layer Control Using Pulsed Discharge Ionization, AIAA 2005-1341, January 2005.
16. Shang, J.S. and Surzhikov, S.T., Magnetoaerodynamic Actuator for Hypersonic Flow Control, AIAA Journal Vol. 43, No. 8, August 2005, pp. 1633-1643.
17. Shang, J.S. Surzhikov, S.T., Kimmel, R. Gaitonde, D.V., Hayes, J.R., and Menart, J., Mechanisms of Plasma Actuators for Hypersonic Flow Control, Progress in Aerospace Sciences, Vol. 41, No. 8, Nov. 2005, pp.642-668.
18. Shang, J.S., Electromagnetic Field of Dielectric Barrier Discharge, AIAA 2005-5182, 36th Plasmadynamics and Laser Conference, Toronto Canada, June 6-9 2005.
19. Boeuf, J.P., Lagmich, Y., Callegari, Th., and Pitchford, L.C., Electro-hydrodynamic Force and Acceleration in Surface Discharge, AIAA 2006-3574., San Francisco, CA, 2006.
20. Lieberman, M.A., and Lichtenberg, A. J., Principles of Plasma Discharges and Materials Processing, John Wiley & Sons, New York, 1994.
21. Hayes, W.D., and Probstein, R.F., Hypersonic Flow theory, Academy Press, 1959.
22. Sutton, G.W. and Sherman, A., Engineering Magnetohydrodynamics, McGraw-Hill, NY, 1965, pp.295-308.
23. Mitchner, M. and Kruger, C.H. Jr. Partially Ionized Gases, John Wiley & Sons, 1973, pp.188-198.
24. Kimmel, R.L., Hayes, J.R., Menart, J.A., and Shang, J.S., Effect of magnetic Fields on Surface plasma Discharges at Mach 5, J. of Spacecraft and Rockets, Vol. 43, No. 6, 2006, pp.1340-1346.
25. Petrusev, A.S., Surzhikov, S.T., and Shang, J.S., A Two-Dimensional Model of Glow Discharge in View of Vibrational Excitation of Molecular Nitrogen, High Temperature, Vol. 44 No. 4, 2006, pp.804-813.
26. von Engel, A. and Steenbeck, M., Elektrische Gasenladungen, Vol. II, Springer, Berlin, 1932.
27. Raizer, Yu. P. and Surzhikov, S.T., Diffusion of Charges along Current and Effective Numerical method of eliminating of numerical Dissipation at Calculations of Glow Discharge, High Temperature, Vol. 28, No. 3, 1990. pp. 324-328.
28. Poggie, J., Plasma-Based Control Shock-Wave/Boundary-Layer Interaction, AIAA 2006-1007, Reno NV. 2006.

29. Surzhikov S.T. and Shang, J.S., The Hypersonic Quasineutral Gas Discharge Plasma in a Magnetic Field, Proceedings third MIT Conference on Computational Fluid and Solid Mechanics, June 14-17, 2005.
30. Rumsey, C., Biedron, R., and Thomas, J., CFL3D: Its History and Some Recent Applications, NASA TM-112861, May 1007.
31. Thomas, J.L., Diskin, B., Brandt, A., Textbook Multigrid Efficiency for Fluid Simulation, Annual Review of Fluid Mechanics, Vol. 35, January 2003, pp.317-340.
32. Shang, J.S., Menart, J., Kimmel, R., and Hayes, J., Hypersonic Inlet with Plasma induced Compression, AIAA 2006-0764, Reno NV, January 2006.
33. Shang, J.S., Menart, J., Kimmel, R., and Hayes, J., Experimental Investigation of Magneto-Fluid-Dynamic Compression in a Cylindrical Inlet, AIAA 2007-0399, Reno NV, January 2007.

Acknowledgment/Disclaimer

This work was sponsored by the Air Force Office of Scientific Research, USAF, under the grant FA9550-05-1-0164. The views and conclusions contained herein are those of the author and should not be interpreted as necessarily representing the official policies or endorsements, either expressed or implied, of the Air Force Office of Scientific Research or the U.S. Government.

Personnel Support during Duration of Grant

Shang, J.S.	Research Professor, Wright State University, Dayton OH
Huang, P.G.	Professor, Wright State University, Dayton OH
Surzhikov, Sergey	Visiting Professor, Russian Academy of Science, Moscow Russia
Hollenbaugh, Sheila	Senior Computing Scientist, Wright State University, Dayton OH
Henderson, Sean	Ph.D. Candidate, Wright State University, Dayton OH
Stanfield, Scott	Ph.D. Candidate, Wright State University, Dayton OH

Publications

I. Journal Articles

1. Surzhikov, S.T., and Shang, J.S., Two-Component Plasma Model for Two-Dimensional Glow Discharge in Magnetic Field, J. Computational Physics, Vol. 199, 2, Sept. 2004, pp. 437-464.

2. Surzhikov, S.T. and Shang, J.S., Viscous Interaction on a Flat Plate with a Surface Discharge in Magnetic Field, High Temperature, Vol. 43, No. 1, 2005, pp.21-31.

3. Shang J.S. and Surzhikov, S.T., Magnetoaerodynamic Actuator for Hypersonic Flow Control, AIAA Journal Vol. 43, No. 8, August 2005, pp. 1633-1643.

4. Shang, J.S., Kimmel, R., Hayes, J., Tyler, C., and Menart, J., Hypersonic Experimental Facility for Magnetoaerodynamic Interactions, J. Spacecraft and Rockets, Vol. 42 No. 5, 2005, pp.780-789.

5. Shang, J.S., Solving Schemes for Computational Magneto-Fluid-Dynamics, Journal of Scientific Computing, Vol. 25, No.1, Oct. 2005, pp.289-306.

6. Shang, J.S., Surzhikov, S.T., Kimmel, R., Gaitonde, D., Menart, J., and Hayes, J., Mechanisms of Plasma Actuators for Hypersonic Flow Control, Progress in Aerospace Sciences, Vol. 41, No. 8, Nov. 2005, pp.642-668.

7. Shang, J.S., Simulating Microwave Radiation of Pyramidal Horn Antenna for Plasma Diagnostics, Communications in Computational Physics, Vol. 1, No. 4, 2006, pp. 677-700.

8. Shang, J.S., Simulating Plasma Microwave Diagnostics, Journal Scientific Computing, Vol. 28, September 2006, pp. 507-532.

9. Kimmel, R.L., Hayes, J.L., Menart, J. A., and Shang, J., Effect of Magnetic Fields on Surface Plasma Discharges at Mach 5, J. Spacecraft & Rockets, Vol. 42, No. 6, 2006, pp.1340-1346.

10. Petrusev, A.S., Surzhikov, S.T., and Shang, J.S., A Two-Dimensional Model for Glow Discharge in View of Vibrational Excitation of Molecular Nitrogen, High temperature, Vol. 44, No. 6, 2006, pp. 804-813.

11. Shang, J.S., Chang, C., and Surzhikov, S.T., Simulating Hypersonic Magneto-Fluid Dynamic Compression, AIAA J. Vol. 45, No. 11, 2007, pp.2710-2720.

12. Shang, J.S., Kimmel, R., Menart, J., and Surzhikov, S.T., Hypersonic Flow Control Using Surface Plasma Actuator, accepted by J. of Propulsion and Power.

II. Conference Papers

1. Shang, J.S., Historical Perspective of Magneto-Fluid-Dynamics, Introduction to Magneto-Fluid-Dynamics for Aerospace Applications, Lecture Series 2004-01, von Karman Institute for Fluid Dynamics, Rhode-ST-Genese Belgium, Oct. 2003.

2. Kimmel, R.L., Menart, J., and Shang, J.S., Design and Implementation of a Magneto-aerodynamic Channel, Introduction to Magneto-Fluid-Dynamics for Aerospace Applications, Lecture Series 2004-01, von Karman Institute for Fluid Dynamics, Rhode-ST-Genese Belgium, Oct. 2003.

3. Shang, J.S., MFD Research in US toward Aerospace Applications, Introduction to Magneto-Fluid-Dynamics for Aerospace Applications, Lecture Series 2004-01, von Karman Institute for Fluid Dynamics, Rhode-ST-Genese Belgium, Oct. 2003.

4. Surzhikov, S.T. and Shang, J.S., Physics of the Direct Current Discharge Interaction with Supersonic Gas Flow, AIAA 2004-0176, 42nd AIAA Aerospace Science Meeting, Reno NV, January 5-8, 2004.

5. Henderson, S., Menart, J., Shang, J.S., Kimmel, R., and Hayes, J., Data Reduction Analysis for a Cylindrical, Double Langmuir Probe Operating in a High Speed Flow, AIAA 2004-0360, 42nd AIAA Aerospace Science Meeting, Reno NV, January 5-8, 2004.

6. Shang, J.S. and Surzhikov, S.T., Magneto-Aerodynamic Interaction for Hypersonic Flow Control, AIAA 2004-0508, 42nd AIAA Aerospace Science Meeting, Reno NV, January 5-8, 2004.

7. Kimmel, R., Hayes, J., Menart, J., and Shang, J.S., Effect of Surface Plasma Discharges on Boundary Layer at Mach 5, AIAA 2004-0509, 42nd AIAA Aerospace Science Meeting, Reno NV, January 5-8, 2004.

8. Shang, J.S., Simulating Microwave Diagnostics for Weakly Ionized Gas, AIAA 2004-0676, 42nd AIAA Aerospace Science Meeting, Reno NV, January 5-8, 2004.

9. Shang, J.S., Simulating Microwave Radiation for Plasma Diagnostics, AIAA 2004-2155, 35th Plasmadynamics and Lasers Conference, Portland OR, 28 June – 1July, 2004.

10. Menart, J., Henderson, S., Shang, J.S., Kimmel, R., and Hayes, J., Study of Surface and Volumetric Heating Effects in a Mach 5 Flow, AIAA 2004-2262, 35th Plasmadynamics and Lasers Conference, Portland OR, 28 June – 1July, 2004.

11. Menart, J., Henderson, S., Shang, J.S., Kimmel, R., and Hayes, J., DC Plasma Discharge Effects on a Mach 5 Flow Between Small Plate Electrodes, AIAA 2004-2264, 35th Plasmadynamics and Lasers Conference, Portland OR, 28 June – 1July, 2004.

12. Shang, J.S., Gaitonde, D., and Updike, G., Simulating Magneto-Aerodynamic Actuator for Hypersonic Flow Control, AIAA 2004-2657, 35th Plasmadynamics and Lasers Conference, Portland OR, 28 June – 1July, 2004.

13. Surzhikov, S.T. and Shang, J.S., Multi-Fluid Models of Weakly Ionized Gas Flows, AIAA 2004-2659, 35th Plasmadynamics and Lasers Conference, Portland OR, 28 June – 1July, 2004.

14. Kimmel, R., Hayes, J., Menart, J., and Shang, J.S., Effect of Magnetic Fields on Surface Plasma Discharges at Mach 5, AIAA 2004-2661, 35th Plasmadynamics and Lasers Conference, Portland OR, 28 June – 1July, 2004.

15. Shang, J.S. and Surzhikov, S.T., Drift-Diffusion Model for Magneto-Fluid-Dynamics Interaction, 3rd International Conference of Computational Fluid Dynamics, Toronto Canada, July 12-16 2004.

16. Updike, G., Shang, J.S., and Gaitonde, D., Hypersonic Separated Flow Control Using Magneto-Aerodynamic Interaction, AIAA 2005-0164, 43rd Aerospace Science Meeting and Exhibit, Reno NV, 10-13 January, 2005.

17. Surzhikov, S.T. and Shang, J.S., Supersonic Flow Around Wing with Localized Surface Gas Discharge, AIAA 2005-0406, 43rd Aerospace Science Meeting and Exhibit, Reno NV, 10-13 January 2005.

18. Shang, J.S., Surzhikov, S.T., Kimmel, R., Gaitonde, D., Menart, J., and Hayes, J., Plasma Actuator for Hypersonic Flow Control, AIAA 2005-0562, 43rd Aerospace Science Meeting and Exhibit, Reno NV, 10-13 January, 2005.

19. Shang, J.S., Diffraction and Refraction in Plasma Diagnostics via Microwave Probing, AIAA 2005-0945, 43rd Aerospace Science Meeting and Exhibit, Reno NV, 10-13 January, 2005.

20. Kimmel, R., Hayes, J., Menart, J., and Shang, J.S., Application of Plasma Discharge Arrays to High-Speed Flow Control, AIAA 2005-0946, 43rd Aerospace Science Meeting and Exhibit, Reno NV, 10-13 January, 2005.

21. Menart, J., Shang, J.S., Atzbach, C., Magoteaux, S., Slagel, M., and Billheimer, B., Total Drag and Lift Measurements in a Mach 5 Flow affected by a Plasma Discharge and a Magnetic Field, AIAA 2005-0947, 43rd Aerospace Science Meeting and Exhibit, Reno NV, 10-13 January, 2005.

22. Surzhikov, S.T. and Shang, J.S., Supersonic Flow Airfoil NACA-0012 with Localized Surface Gas Discharge, 6th Aeroplasma Dynamics Conference, Moscow Russia, May 2005.

23. Surzhikov, S.T. and Shang, J.S., The Quasineutral Gas Discharge Plasma in Strong Magnetic Field and Hypersonic Gas Flow, 6th Aeroplasma Dynamics Conference, Moscow Russia, May 2005.

24. Menart, J.A. and Shang, J.S., Investigation of Heating and Lorentz Force Effects Caused by a Plasma and a Magnetic Field in a Mach 5 Flow, AIAA 2005-4783, 36th Plasmadynamics and Laser Conference, Toronto Canada, June6-9 2005.

25. Shang, J.S. and Chang, C.L., Magneto-Aerodynamic Interaction over Airfoil, AIAA 2005-5179, 36th Plasmadynamics and Laser Conference, Toronto Canada, June6-9 2005.

26. Shang, J.S., Electromagnetic Field of Dielectric Barrier Discharge, AIAA 2005-5182, 36th Plasmadynamics and Laser Conference, Toronto Canada, June6-9 2005.

27. Petrusev, A.S., Surzhikov, S.T., and Shang, J.S., Some Peculiarity of Direct Current Discharge for Aerospace Applications, AIAA 2005-5305, 36th Plasmadynamics and Laser Conference, Toronto Canada, June6-9 2005.

28. Surzhikov, S.T. and Shang, J.S., The Hypersonic Quasineutral Gas Discharge Plasma in a Magnetic Field, Proceedings third MIT Conference on Computational Fluid and Solid Mechanics, June 14-17, 2005, pp1004-1005.

29. Stanfield, S., Menart, J., and Shang, J., Application of a Spectroscopic Measuring Technique to Plasma Discharge in Hypersonic Flow, AIAA 2006-0559, Reno NV, January 2006.

30. Shang, J.S., Electromagnetic Perturbation to Hypersonic Viscous-Inviscid Interaction, AIAA 2006-0709, Reno NV, January 2006.

31. Kimmel, R., Hayes, J., Crafton, J., Fonov, S., Menart, J., and Shang, J.S., Surface Discharges for High-Speed Boundary-Layer Control, AIAA 2006-0710, Reno NV, January 2006.

32. Shang, J.S., Menart, J., Kimmel, R., and Hayes, J., Hypersonic Inlet with Plasma induced Compression, AIAA 2006-0764, Reno NV, January 2006.

33. Menart, J., Stanfield, S., Shang, J.S., Kimmel, R., and Hayes, J., Study of Plasma Electrode Arrangements for Optimum Lift in a Mach 5 Flow, AIAA 2006-1172, Reno NV, January 2006.

34. Surzhikov, S.T. and Shang, J.S., Glow Discharge in Flow of Neutral Gas and External Magnetic Field, AIAA 2006-1371, Reno NV, January 2006.

35. Petrusev, A., Surzhikov, S.T., and Shang, J.S., Chemical Process in air Glow Discharge for Aerospace Applications, AIAA 2006-1460, Reno NV, January 2006.

36. Shang, J.S., Chang, C.L., and Surzhikov, S.T., Simulating Hypersonic Magneto-Fluid-Dynamic Compression, AIAA 2006-2889, San Francisco CA, June 2006.

37. Petrusev, A., Surzhikov, S.T., and Shang, J.S., Numerical Algorithm for Modeling Chemically Active Glow Discharge in Air, AIAA 2006-2906, San Francisco CA, June 2006.

38. Surzhikov, S.T. and Shang, J.S., "Anomalous" behavior of Glow Discharge in External Magnetic Field, AIAA 2006-3384, San Francisco CA, June 2006.

39. Shang, J.S., Computing Simulation of Hypersonic Magneto-Fluid-Dynamic Interaction, Fourth International Conf. on CFD, Ghent Belgium, July 10-14, 2006.

40. Shang, J.S., Menart, J., Kimmel, R., and Hayes, J., Experimental Investigation of Magneto-Fluid-Dynamic Compression in a Cylindrical Inlet, AIAA 2007-0399, Reno NV, January 2007.

41. Petrusev, A.S., Surzhikov, S.T., and Shang, J.S., 3D Modelling of Glow Discharge with Physical-Chemical Kinetics, AIAA 2007-0825, Reno NV, January 2007.

42. Surzhikov, S.T. and Shang, J.S., Normal Microwave Glow Discharge in Transversal Magnetic Field, AIAA 2007-0992, Reno NV, January 2007.

43. Surzhikov, S.T. and Shang, J.S., Plasmadynamics of Glow Discharges in Hypersonic Internal Flows, AIAA 2007-0994, Reno NV, January 2007.

44. Yan, H., Gaitonde, D., and Shang, J.S., Investigation of Localized Arc Filament Plasma Actuator in Supersonic Boundary Layer, AIAA 2007-1234, Reno NV, January 2007.

45. Shang, J.S. and Chang, C.L., Hypersonic Magneto-Fluid-Dynamic Compression in Cylindrical Inlet, AIAA 2007-3885, Miami FL., June 2007.

46. Yan, H., Gaitonde, D., and Shang, J.S., Numerical Investigation of Pulsed Thermal Perturbation in Supersonic Boundary Layer, AIAA 2007-3885, Miami FL., June 2007.

47. Shang, J.S., Some Flow-Structure Features of Scramjet Isolator, AIAA 2008-0772, Reno NV, January 2008.

48. Shang, J.S., Surface Direct Current Discharge for Hypersonic Flow Control, AIAA 2008-1352, Reno NV, January 2008.

49. Shang, J.S., Huang, P.G., Yan, H., and Surzhikov, S.T., Electrodynamics of Direct Current Discharge, AIAA 2008-1101, Reno NV, January 2008.

50. Yan, H., Gaitonde, D.V., and Shang, J.S., Stability Analysis of Thermal Bump in Supersonic Flow, AIAA 2008-1096, Reno NV, January 2008.

51. Surzhikov, S.T. and Shang, J.S., Kinetic Models Analysis for Super-Orbital Aerophysics, AIAA 2008-1278, Reno NV, January 2008.

Honors & Awards Received

USAF Basic Research Award, 1986
Fellow of AIAA, 1993
Exception Civilian Service Award, 2001
AIAA Plasmadynamics and Laser Award, 2004

AFRL Point of Contact

Dr. Donald B. Paul, AFRL/VA WPAFB, OH 937-255-7329, met weekly.
Dr. Alan Garscadden, AFRL/PR WPAFB, OH 937-255-2246, interacted monthly and actively participated in Window in Science Seminars.
Dr. Roger Kimmel, AFRL/VAAA WPAFB, OH 937-255-8295, interacted weekly.
Dr. Datta V. Gaitonde, AFRL/VAAC WPAFB, OH 937-904-4031, interacted weekly.
Messrs. Michael Zeigler and James Hayes, AFRL/VAAI WPAFB, OH 937-656-6307 and 937-255-1260, interacted and met weekly.

Transitions

Three technical transitions have been initiated and completed during the reporting period. The first two activities are in the category of knowledge transfer and the third activity is considered to be a direct USAF mission support.

The concept and potential practical applications of the plasma actuator that perform as a virtual leading edge strake and a variable geometry inlet of a hypersonic vehicle have been directly transferred to the Air Vehicle Directorate of Air Force Research Laboratory (AFRL/VA). In the virtual leading edge application, the magneto-fluid-dynamic interaction on a fixed control surface has demonstrated an equivalent pitching angle of seven degrees at a free-stream Mach number of 5.15. The basic research results also guide a research and development initiative for improving hypersonic vehicle performance and address the fundamental compatibility issue of magneto-fluid-dynamics compression within a rectangular and cylindrical inlet with high lift-to-drag hypersonic vehicles. Although all computational and experimental simulations are conducted at a Mach number of 5.15, according to classic theory the flow control effectiveness will increase with increasing flight speed. More importantly, the experimental effort also develops a validating database for numerical simulation of magneto-aerodynamic actuator for hypersonic flow control. Points of contact at the AFRL/VA are Dr. D. Paul, AFRL/VA 937-255-7329, Michael Zeigler, AFRL/VAAI, 937-656-4169, Dr. Roger Kimmel AFRL/VAAA, 937-255-8295, James Hayes AFRL/VAAI, 937-255-1260, and Dr. Datta Gaitonde AFRL/VAAC, 937-904-4031.

The newly acquired interdisciplinary computational simulation capability for magneto-fluid-dynamic interaction and the basic knowledge of ionization modeling via electrons collision have been transferred to National Institute of Aerospace, NASA Langley Research Center. Point of contact at the NASA Langley Research Center is Dr. C. L. Chang, 757-864-5369.

The most recent technical transition from the present basic research program is the micro aerial vehicle (MAV) initiative that will be supported by the Chief Scientist Innovative Research Fund (CSIRF) of AFRL/VA. The MAV project integrates the SAE winning micro aircraft platform of Wright State University with a plasma flow control mechanism. Several unique plasma-based lateral flight control implementation will be introduced to improve flight characteristic of the basic fly-wing configuration. Point of contact at the AFRL/VA is Denis Mrozinski AFRL/VAAA 937-255-3610.

New Discoveries

The rather simple hypersonic rectangular and cylindrical inlet configurations have been found to generate complex shock-wave structures. Upstream to the interception of MFD induced shock waves, eight triple points are observed on the envelope shock of the rectangular inlet. The shock wave structure of the cylindrical inlet is simpler but the focus of the conical shock that originates from the leading edge becomes the bifurcation point from a regular to Mach reflection. These findings may have significant impact to the isolator aerodynamic performance of scramjet. Equally important the Mangler scaling of the axisymmetrical configuration has reduced MFD compression by shrinking the boundary-layer displacement thickness.

Both experimental and computational investigations have shown that an externally applied magnetic field suppresses the plasma generation via electron collision. In an electric field intensity dominated phenomenon, the Hall parameter actually reduces the effective electric potential. A quantification of the phenomenon is being verified by a drift-diffusion ionization model.

Consultative and Advisory Functions:

The principal investigator of the research grant is retained by the AFRL as an emeritus scientist to rejuvenate the aerodynamic experimental programs. He also continues his role as a member of the AIAA Plasmadynamics and Laser Technical Committee since April 1992.

NASA NIA/LaRC (National Institute of Aerospace, NASA, Langley Research Center) invited the principal investigator of the present research grant to be a visiting research scholar for their plasmadynamic R&D programs (Research Cooperative Agreement, NCC-1-02043).